

1 **MM5 v3.6.1 and WRF v3.5.1 model comparison of standard**
2 **and surface energy variables in the development of the**
3 **planetary boundary layer**

4
5 Cari-Sue M. Wilmot, Bernhard Rappenglück, Xiangshang Li, Gustavo Cuchiara

6
7 Department of Earth and Atmospheric Sciences, University of Houston, Houston, Texas,
8 USA

9
10 Correspondence to: B. Rappenglück (brappenglueck@uh.edu)

11
12
13 **Abstract**

14 Air quality forecasting requires atmospheric weather models to generate accurate
15 meteorological conditions, one of which is the development of the planetary boundary layer
16 (PBL). An important contributor to the development of the PBL is the land-air exchange
17 captured in the energy budget as well as turbulence parameters. Standard and surface energy
18 variables were modeled using the fifth-generation Penn State/National Center for
19 Atmospheric Research mesoscale model (MM5), version 3.6.1, and the Weather Research and
20 Forecasting (WRF) model, version 3.5.1 and compared to measurements for a southeastern
21 Texas coastal region. The study period was August 28 - September 01, 2006. It also included
22 a frontal passage.

23 The results of the study are ambiguous. Although WRF does not perform as well as MM5 in
24 predicting PBL heights, it better simulates energy budget and most of the general variables.
25 Both models overestimate incoming solar radiation, which implies a surplus of energy that
26 could be redistributed in either the partitioning of the surface energy variables or in some
27 other aspect of the meteorological modeling not examined here. The MM5 model consistently
28 had much drier conditions than the WRF model, which could lead to more energy available to
29 other parts of the meteorological system. On the clearest day of the study period MM5 had
30 increased latent heat flux, which could lead to higher evaporation rates and lower moisture in
31 the model. However, this latent heat disparity between the two models is not visible during
32 any other part of the study. The observed frontal passage affected the performance of most of
33 the variables, including the radiation, flux, and turbulence variables, at times creating
34 dramatic differences in the r^2 values.

35

36 **1 Introduction**

37 Due to a combination of complex chemical and meteorological interactions, Houston suffers
38 from air pollution problems. Metropolitan traffic and a bustling refinery industry generate
39 primary pollutants as well as precursors for secondary pollutants such as ozone. Despite the
40 simple topography of the area, Houston's proximity to the Gulf of Mexico leads to a complex
41 meteorological system that is influenced by both synoptic-scale and local land-sea breeze
42 circulations. Various studies examining the interaction between these forcings have often
43 noted that some of the most severe ozone exceedance days have occurred during stagnant
44 periods when local and synoptic forces have clashed (Banta et al., 2005; Rappenglück et al.,
45 2008; Langford et al., 2010; Tucker et al., 2010; Ngan and Byun, 2011).

46 In order to alert people to potentially health-threatening pollution levels, numerical weather
47 prediction (NWP) models coupled to chemical models are used to predict the weather and its
48 subsequent effect on atmospheric chemistry for the area. Two such models are the fifth-
49 generation Penn State/National Center for Atmospheric Research mesoscale model (MM5;
50 Grell et al., 1994) and the Weather Research and Forecasting (WRF) model (Skamarock et al.,
51 2008). The MM5 model has been used extensively to simulate meteorological inputs for use
52 in air quality models such as the Community Multiscale Air Quality (CMAQ; Byun and
53 Schere, 2006) model.

54 Some studies, such as that done by Mao et al. (2006), have examined MM5 in the capacity of
55 a coupled model, endeavoring to understand how changing the meteorological forcings affects
56 the atmospheric chemistry output. Similarly, Ngan et al. (2012) looked at MM5 performance
57 in connection with the CMAQ model ozone predictions. Other studies, such as was done by
58 Zhong et al. (2007), have instead looked directly at MM5 output in order to better understand
59 the meteorological parameterizations most appropriate for the local area.

60 Although MM5 is still being used for research purposes, the next-generation WRF model is
61 now in general use. Developers of MM5 physics have imported or developed improved
62 physics schemes for WRF, such as discussed in Gilliam and Pleim (2010), who found that the
63 errors in all variables studied across the domain were higher in MM5 than in either WRF run
64 with a similar configuration or the WRF run with a more common configuration. Their final
65 conclusion was that the WRF model was now at a superior level to MM5 and should therefore
66 be used more extensively, especially to drive air quality models. Hanna et al. (2010) tested the
67 Nonhydrostatic Mesoscale Model core for WRF (WRF-NMM) against MM5 for boundary
68 layer meteorological variables across the Great Plains, and Steeneveld et al. (2010) used

69 intercomparisons between MM5 and WRF to examine longwave radiation in the Netherlands.
70 Both of these studies came to the conclusion that in general, WRF outperformed MM5.
71 The common parameters examined in all of these previous studies are the planetary boundary
72 layer (PBL) schemes and land surface models (LSMs), because in spite of improvements in
73 predictions of standard atmospheric variables such as surface temperature and wind fields,
74 characteristics of the PBL, especially PBL height, continue to elude modelers. For example,
75 when Borge et al. (2008) did a comprehensive analysis of WRF physics configurations over
76 the Iberian Peninsula, PBL height estimates for two observation sites were poor at night and
77 during the winter, which are classically periods of stable boundary layer development. Other
78 studies have found similar performance with PBL height (Wilczak et al., 2009; Hanna et al.,
79 2010; Hu et al., 2010).

80 Although many of these studies examine the sensitivity of WRF to PBL scheme and LSMs,
81 not as much attention has been given to evaluating the effects of the energy balance variables
82 generated by these various schemes. The complex interaction between latent and sensible
83 heat, radiation and ground flux all affect the performance of meteorological variables, which
84 in turn affect boundary layer properties such as PBL height. Analyzing the performance of
85 these variables within a model should give further insight into the mechanisms that affect
86 boundary layer properties, but these energy balance variables are not as commonly evaluated
87 in the model because of a lack of observations.

88 Variations of the PBL height play an important role in air quality. Studies performed during
89 the first and second Texas Air Quality Study (TexAQS-2000, TexAQS-II) have noted an
90 increase in ozone after a frontal passage in the Houston area (Wilczak et al., 2009;
91 Rappenglück et al., 2010; Tucker et al., 2010). This study is conducted to determine how well
92 the MM5 and WRF models simulate PBL height, variables affecting its development, and
93 standard atmospheric variables for a frontal passage during TexAQS-II.

94

95 **2 Observational data, models, and statistical analysis**

96 **2.1 Location**

97 The focus of this study is the University of Houston Coastal Center (UH-CC), which is
98 located near the Gulf of Mexico coast (29°23'16.67" N, 95°02'29.09" W) and is surrounded by
99 approximately 200 acres (0.81 km²) of prairie grass (Figure 1). This location was selected
100 both because it is the location of previous field studies (Clements et al., 2007; Zhong et al.,
101 2007) and is clear of surrounding structures that would interfere with the natural
102 meteorological processes. Its micrometeorological setup is comprehensively described in

103 Clements et al., 2007. Most of the measurements used in this study were taken from 10 m, 2
104 m, or at the surface. Using a parameterized Lagrangian back trajectory footprint model
105 according to Kljun et al. (2004) it is possible to estimate maximum impact distances and 90%
106 impact boundaries of the footprint affecting the observations (available at
107 <http://footprint.kljun.net/>). Typical values for the daytime surface friction velocity u^* are
108 about 0.3-0.5 m/s, for the standard deviation of the vertical velocity fluctuations about 0.7-0.9
109 m/s. The roughness length is estimated to be 0.05 m. For 10 m measurements this yielded
110 maximum impact distances of 85-100 m and 90% impact boundaries of 230-285 m, which is
111 well within the surrounding prairie grass area. Most of the modeling and observation data was
112 extracted from this location with the exception of the radiosondes, which were launched from
113 the UH main campus (Rappenglück et al., 2008), and wind fields for the inner WRF domain,
114 which were provided by the Texas Commission on Environmental Quality (TCEQ)
115 Continuous Ambient Monitoring Stations (CAMS) in the surrounding area.

116

117 **2.2 Observational data**

118 **2.2.1 Measurement Tower instrumentation**

119 During the study period August 28 - 31, 2006, both standard and energy budget surface
120 variables were being measured (Table 1). Instrumentation included an R.M. Young 5103
121 anemometer to capture 10-mean wind speeds (WDIR10) and directions (WSPD10), a
122 Campbell Scientific, Inc. (CSI) CS-500 probe for 2-m temperature (TEMP2) and 2-m water
123 vapor mixing ratio (Q2), and a Kipp & Zonen CNR1 four-component net radiometer to
124 capture incoming shortwave (SWDOWN), incoming longwave (LWDOWN), outgoing
125 shortwave (SWUP), and outgoing longwave radiation. A three-dimensional (3-D) sonic
126 anemometer (R.M. Young 8100) was used to determine sensible heat flux (SHFLUX) and in
127 combination with a collocated LI-COR 7500 open-path infrared gas analyzer to collect data
128 about latent heat flux (LHFLUX). Ground fluxes (GRNDFLUX) were measured using
129 Radiation and Energy Balance System (REBS) soil heat flux plates.

130 Measurements were taken at a frequency of 1 Hz and averaged to 1 minute (TEMP2, Q2,
131 WSPD10, WDIR10) and 10 minutes (SWDOWN, LWDOWN, SWUP, SHFLUX, LHFLUX,
132 GRNDFLUX). All measurements were then averaged to one hour to compare to the hourly
133 model data.

134

135 **2.2.2 Radiosonde data**

136 Radiosondes were not directly measured at the UH-CC during this study period, but were
137 regularly launched from the UH main campus approximately 40 km away. RS-92 GPS sondes
138 were used (Rappenglück et al., 2008). The difference in potential temperature vertical lines
139 between the grid point representing the UH-CC and the UH was zero, which gave confidence
140 that PBL heights measured at UH provide a reasonable approximation for model comparison
141 at the UH-CC. Launches were performed at 0600 CST and 1800 CST for the first two days of
142 the study period, and more were launched during the final two days of the study (Table 2).
143 PBL heights were determined to be the height at which potential temperature begins to
144 increase (Rappenglück et al., 2008). The first radiosonde launch was discarded for purposes
145 of statistical analysis because it corresponded to the model initialization time step, which had
146 a value of 0.

147

148 **2.3 WRF model**

149 The WRF model used for the simulation was the Advanced Research WRF (WRF-ARW)
150 model version 3.5.1 with the following physics configuration: WSM-3 class simple ice
151 microphysics scheme (Hong et al., 2004), Dudhia shortwave radiation scheme (Dudhia,
152 1989), Rapid Radiative Transfer Model (RRTM) longwave radiation scheme (Mlawer et al.,
153 1997), Yonsei University (YSU) (Hong et al., 2006) PBL scheme, and the MM5 land surface
154 scheme (Noah LSM). In past air quality studies in Houston we used YSU and found
155 promising results (Czader et al., 2013), and recent intercomparisons with other PBL schemes
156 for the same area showed that YSU simulates vertical meteorological profiles as satisfactorily
157 as the Asymmetric Convective Model version 2 (ACM2); the Mellor–Yamada–Janjic (MYJ)
158 and Quasi-Normal Scale Elimination (QNSE), but may be the best to replicate vertical mixing
159 of ozone precursors (Cuchiara et al., 2014). The cumulus scheme is set to be identical to the
160 MM5 one, which is described below.

161 The model was run on three nested domains using 1-way nesting (Figure 2). The horizontal
162 grid scales were the 36-km CONUS domain, 12-km eastern Texas domain, and the 4-km
163 Houston-Galveston-Brazoria domain. All simulation results are taken from the 4-km domain
164 grid cell centered over the UH Coastal Center (Figure 1) and is thus a point-to-grid cell
165 comparison. The 90% boundaries of the footprint of the observations fall within this grid cell.
166 No Observational nudging was used to avoid any potential effects introduced by nudging
167 procedures. The model was initialized on 0000 UTC 28 AUG 2006 and ended on 2300 UTC
168 SEP 1 2006. The North America Mesoscale (NAM) model was used as meteorological input.

169

170 **2.4 MM5 model**

171 In order to examine any improvements made from the MM5 to WRF simulations, data
 172 extracted from an MM5 simulation was used for a baseline comparison for the Houston case
 173 (Table 3). Similarly to previous studies by Ngan et al. (2012) for TexAQS-II in Houston, we
 174 applied MM5, version 3.6.1. The physics options included the Medium-Range Forecast
 175 (MRF; Hong and Pan, 1996) PBL scheme, Noah LSM, simple ice microphysics scheme, and
 176 RRTM radiation scheme. No observational nudging was used. The same horizontal grid scale
 177 as for WRF was used. The cumulus parameterization is set to: Grell-Devenyi Ensemble
 178 scheme (Grell and Devenyi 2002) for 36-km domain, Kain-Fritsch scheme (Kain, 2004) for
 179 12-km and none for 4-km domain. The choice of no cumulus in 4-km is to suppress the
 180 unwanted fake thunderstorms frequently popping up in the model.

181

182 **2.5 Differences between the WRF and MM5 configuration.**

183 The differences between the two models' configurations are the cloud scheme and the land
 184 analysis used for the initialization. The EDAS and NAM land surface datasets are similar and
 185 use similar observational techniques for data interpolation, but the EDAS runs every three
 186 hours, which allows for higher-resolution temporal interpolation than the NAM data, which
 187 only runs every six hours (EDAS Archive Information, National Weather Service
 188 Environmental Center). Using a more high-resolution dataset should lead to better first-guess
 189 and ongoing simulations in MM5.

190

191 **2.6 Statistical Analysis**

192 **2.6.1 Calculated Statistics**

193 For the purposes of this study, the coefficient of determination (r^2), the root mean square error
 194 (RMSE) and bias are displayed. The RMSE describes the magnitude of the difference
 195 between predicted and observed values. The r^2 indicates the proportionate amount of variation
 196 in the response variable y explained by the independent variables x in the linear regression
 197 model. The larger r^2 , the more variability is explained by the linear regression model. The r^2
 198 was calculated using a linear model in Matlab. The bias and RMSE was determined as
 199 follows:

$$200 \quad BIAS = \frac{1}{n} \sum (Y' - Y) \quad (1)$$

$$201 \quad RMSE = \sqrt{\frac{1}{n-1} \sum (Y' - Y)^2} \quad (2)$$

202

203 where n is the number of values, Y' is the modeled value, and Y is the observed value.

204

205 **2.6.2 Determination of additional statistic groups**

206 Hourly values were collected from 0000 August 28-1700 September 01, resulting in 114 data
207 points (Table 4). Biases and r^2 values were evaluated for the complete data set as well as for
208 diurnal and frontal clusters. For the diurnal statistics, daytime referred to any data between
209 0600 CST and 1800 CST. Rappenglück et al. (2008) discussed the frontal passage that
210 occurred during this period, which occurred during the evening of August 29. An examination
211 of the meteorology shows that generally southerly winds gave way to sustained northerly
212 winds on August 29 around 1830 CST, indicating this frontal passage. For the purposes of
213 this study, the prefrontal period runs from 0000 CST August 28 to 1900 CST August 29, and
214 the postfrontal period runs from 2000 CST August 29 to 1700 CST September 01.

215

216 **3. Results and discussion**

217 **3.1. Standard meteorological variables**

218 **3.1.1 Temperature**

219 WRF has the highest r^2 for all of the study period as well as when the data is separated into
220 daytime, nighttime, prefrontal, and postfrontal time periods (Table 5). The largest differences
221 between the WRF and MM5 model in the r^2 value occur at night and during prefrontal
222 conditions, both of which have differences of 0.53. However, the nighttime r^2 value for MM5
223 was the smallest at 0.04, which reflects the variability in the nighttime temperature modeling.
224 The WRF model has a higher nighttime r^2 value of 0.57, but this value also represents the
225 smallest r^2 value for the model, which implies that both models have difficulty getting
226 nighttime temperatures correct. Batching the data into prefrontal and postfrontal groups had
227 little effect on the r^2 values for WRF, but led to increased values in both of the MM5 models.
228 WRF and MM5 have about the same magnitude bias for the entire study period, but WRF has
229 larger biases for the daytime and nighttime, while WRF has lower biases for prefrontal period,
230 and in particular postfrontal period. The overall biases for all of the simulations are relatively
231 low but both WRF and MM5 underestimate temperatures by about half a degree during the
232 day and overestimate temperatures by about one and a half degree at night for the entire study
233 period (Table 5). These biases could possibly be attributed to too much moisture in the
234 models, which would suppress temperature amplitudes. This warm nighttime bias is
235 especially evident on the nights of August 30 and August 31 (Figure 3). These biases could be
236 the product of too much moisture in the model, which would lead to less suppressed

237 temperature peaks. Another possibility is that there is too much nighttime surface energy in
238 the model, which could lead to increased nighttime temperatures. Also, higher modeled
239 nighttime winds could lead to a well-mixed nighttime atmosphere, which would prevent
240 temperatures from dropping as low as they should in the model.

241 Steeneveld et al. (2010) noted that both of the models have difficulty simulating nighttime
242 temperatures. That same study also mentioned that the MM5 warming and cooling trends
243 tended to lag behind the observations, which is visible in the time series for the first half of
244 this study as well (Figure 3). The WRF model simulation does not have this same time lag.

245

246 **3.1.2 Water vapor**

247 WRF r^2 values for water vapor are lower than the MM5 r^2 values (Table 5). The overall r^2
248 values were highest for MM5, while the daytime r^2 values were highest for both WRF and
249 MM5. MM5 had the highest overall and postfrontal values. Both of the models saw low r^2
250 values prior to the frontal passage, which only increased for MM5 following the frontal
251 passage. WRF had lowest values postfrontal and prefrontal values. The water vapor mixing
252 ratio r^2 values are relatively high for MM5 although they are lower than the temperature r^2
253 values. For WRF these values are consistently lower than the temperature r^2 values. Daytime
254 water vapor mixing ratio tended to be higher than the overall r^2 , while nighttime water vapor
255 r^2 values were slightly lower than the overall r^2 for MM5, but significantly lower for WRF.
256 MM5 overall, daytime, and nighttime r^2 values were higher than WRF. This is even more
257 evident for the prefrontal and postfrontal conditions.

258 Table 5 shows that both models underestimated moisture for the entire study period with dry
259 biases of 1.44 g/kg and 2.61 g/kg for WRF and MM5, respectively. During the day, this dry
260 bias increases for both WRF and MM5 to 1.47 g/kg and 2.81 g/kg. However, at night, the dry
261 bias decreases to 1.40 g/kg and 2.36 g/kg for WRF and MM5, respectively. Zhong et al.
262 (2007) modeled water vapor at the UH-CC and saw biases of 1.38 during the day, -0.63 at
263 night, and 0.37 for the overall value, which indicated overestimation of moisture during the
264 day and underestimation at night. The difference in the two models' moisture bias could be
265 attributed to the different land initialization schemes used for the two models, but in either
266 case temperature performance during the entire study period appears to be affected by more
267 than the water vapor mixing ratios.

268 For the two days following the frontal passage, the models' temperature and water vapor
269 mixing ratio biases appear to be more coupled. WRF underestimates daytime temperature
270 with a bias of -3.31°C and could correspond to a moist bias of -3.05 g/kg, while MM5 slightly

271 overestimates daytime temperature with a bias of 0.12°C and could correspond to a moist bias
272 of -2.65 g/kg . The days following the frontal passage were mostly cloudless, so temperature
273 may be more directly affected by moisture. The fact that following the frontal passage the
274 conditions are more dry could also be a contributing factor, as the observed water vapor
275 mixing ratio dropped by approximately 4 g/kg for the remainder of the study period (figure
276 not shown). Moisture bias effects could be magnified in light of much smaller moisture
277 values.

278 For the two nights following the frontal passage, both models' dry biases are relatively close
279 to the mean nighttime biases of the entire study period, but temperature biases are not
280 proportional to these changes. The nighttime biases decrease by 0.84 g/kg and 0.09 g/kg for
281 WRF and MM5, respectively, but both models clearly overestimate temperature on the nights
282 of August 30 and August 31 (Figure 3). For the entire study period, the models have too warm
283 nighttime biases of 1.46°C and 1.33°C for WRF and MM5, respectively; these warm biases
284 increase to 2.22°C and 2.61°C for those two nights.

285

286 **3.1.3 Wind speed**

287 Wind speeds had generally low r^2 values, with the highest overall r^2 being the MM5
288 simulation using EDAS (Figure 3). Separating data into day and nighttime values did not
289 increase the r^2 values; in fact, both day and nighttime r^2 were lower than the overall values for
290 both of the models. While the MM5 model bias was relatively small and slightly
291 underestimated during the daytime, the WRF model overestimated with a much higher
292 magnitude. Both models have the largest biases at night when wind speeds are overestimated,
293 and with the highest overestimation occurring by the WRF model. Ngan et al. (2012) mention
294 that modeled MM5 winds persisted for hours after the observed winds had died down at
295 sunset. A similar trend is visible for a few nights of this study period in MM5, but is most
296 clearly evident in the WRF model.

297 Wind speed r^2 values were equally low for both prefrontal and postfrontal conditions.
298 However, clustering data by frontal condition led to having at least one higher r^2 value for
299 each model than for all of the data combined (Table 5). In WRF, the prefrontal value was
300 lower than the postfrontal value, and this was the lowest prefrontal value among the models.
301 The MM5 model postfrontal value was higher. Prefrontal biases are low for MM5, but
302 appreciably high for WRF. For both models biases increase in the postfrontal environment.
303 Tucker et al. (2010) found that daytime winds tended to be higher and be more southerly
304 following strong low level jet (SLLJ) nights, and they were weaker and either northerly or

305 stagnant following weak LLJ (WLLJ) nights. Although it slightly overestimates wind speeds,
306 WRF is able to better capture the post-SLLJ conditions on August 28 which correspond to
307 prefrontal conditions. However, WRF persists in generating high winds on the days following
308 two WLLJ nights (August 31 and September 1), which correspond to postfrontal conditions
309 and leads to a much higher bias. The MM5 model does not suffer from high bias to the same
310 extent, but it also tends to overestimate more following the postfrontal conditions
311 corresponding to the post-WLLJ scenario.

312

313 **3.1.4 Wind direction**

314 Wind direction r^2 values were generally low for the entire study period and at nighttime for
315 both models, and only reach approximately 0.50 during the daytime (Table 5). Houston's
316 proximity to the Gulf generally means that there is a strong diurnal cycle as the temperature
317 difference between the land and the water creates surface pressure gradients. This cycle tends
318 to manifest itself in strong southerly winds during the daytime and more northerly winds in
319 the evening and at night. However, during this time period the frontal passage led to more
320 persistent northerly winds, which might have interfered with the normal cycle of the models
321 (Figure 3). The prefrontal and postfrontal r^2 values are both with values at or near 0.30 for
322 MM5 and below 0.10 for WRF. During the study period, wind direction was variable as the
323 front and the daytime wind cycle came into contact.

324 The magnitudes for the overall, daytime, and nighttime biases were an order of magnitude
325 larger for WRF than for MM5 in most cases. Wind direction for the entire study was
326 underestimated by 21.48 degrees and 2.41 degrees in WRF and MM5, respectively, which
327 means that the wind directions were in the same quadrant, but for WRF started having more
328 of an orthogonal wind component. During the daytime these bias magnitudes increase for
329 both models. This could possibly be related to the frontal passage, especially during the day
330 when the frontal passage and the land-sea breeze cycle led to stagnant air conditions and wind
331 directions were variable. Southerly winds are associated with moist, ocean air, while north
332 and northwesterly winds are associated with drier, continental air, so the direction of the wind
333 in the models could relate to the level of water vapor mixing ratio found in the models.

334

335 **3.2 Energy budget variables**

336 **3.2.1 Radiation**

337 Longwave outgoing radiation as only available at the top of the atmosphere, not at the
338 surface, for both WRF and MM5. Thus it cannot be adequately compared with surface

339 observations. Therefore this variable was removed from the study analysis, and only the other
340 three components of radiation were studied (Table 5).

341

342 *Incoming-longwave radiation*

343 The r^2 values for longwave radiation are often lower than for either temperature or water
344 vapor mixing ratio, but are still relatively high (Table 5). WRF has a higher r^2 during the
345 daytime than overall, while MM5E is slightly lower than the overall value during the daytime.
346 The overall and daytime WRF r^2 values are about the same as the MM5E values, but at night,
347 MM5 has a slightly higher r^2 than the WRF model. Both models have relatively low nighttime
348 r^2 values compared to either daytime or overall values.

349 Both models overestimate incoming longwave radiation with the largest overestimations
350 occurring at night. WRF has larger biases than MM5 for day and nighttime. However, the
351 minimum longwave radiation value recorded during this time period was $\sim 371 \text{ W/m}^2$. Even
352 the largest bias (8 W/m^2) only represents a 2% overestimation of incoming longwave
353 radiation.

354 There is a slight time lag in both the cooling and the warming trends for the longwave
355 radiation for both models, but they both also attempt to capture the drop in radiation following
356 the frontal passage (Figure 4). Both of the models overestimated; prefrontal conditions
357 produced the largest bias. In MM5 there is an almost 50% drop in bias from the prefrontal to
358 postfrontal data cluster, and a WRF even changed to underestimation. WRF had the lowest
359 overall, but highest frontal cluster biases.

360

361 *Incoming/outgoing shortwave radiation*The models treat outgoing radiation as a direct
362 decrease caused by albedo. Therefore, both incoming and outgoing shortwave radiation are
363 driven to 0 after sunset, leading to the "-" found in the tables for nighttime values. For
364 outgoing radiation, the WRF model performs better than the MM5 model, which has very
365 small r^2 values during the daytime (Table 5). These small r^2 values are most likely the result
366 of the overestimations found during the early part of the study period when MM5
367 overestimates outgoing shortwave radiation by as much 337 W/m^2 (Figure 4) and results in
368 daytime biases of 60 W/m^2 . While the overall bias in the WRF model is slightly
369 overestimated, it is overestimated in MM5 with a magnitude of 33 W/m^2 .

370 For the first two days of the study period, incoming solar radiation (SWDOWN) did not reach
371 maximum insolation peaks, possibly due to scattered cloud cover. Following the frontal
372 passage on August 29, cloud cover began to dissipate as observed incoming solar radiation

373 began to increase, reaching maximum insolation on the afternoon of August 31 before again
374 devolving on September 01. However, both models moved too soon in developing maximum
375 insolation (Figure 4).

376 During the daytime for the entire study period, both models tended to overestimate
377 SWDOWN (Table 5). However, for the two clearest days of the study period, both WRF and
378 MM5 overestimated incoming solar radiation by 75.5 W/m^2 and 52.9 W/m^2 , respectively.
379 While these values drop to 16.25 W/m^2 and 17.27 W/m^2 on the clearest day of the study, both
380 models continue to overestimate incoming solar radiation. This excess energy in the models
381 could appear as overestimations in the energy flux partitions for sensible, latent, and ground
382 flux.

383 Incoming radiation r^2 values are generally higher than the outgoing values for both of the
384 models, but daytime r^2 values are still lower than the overall r^2 values (Table 5). WRF
385 performs better than the MM5 model for all values. Both models tend to overestimate the
386 radiation, but the magnitudes of the biases for incoming radiation are smaller for MM5, while
387 the magnitudes of the biases for outgoing radiation are smaller for WRF (Table 5). Similar to
388 outgoing radiation, the magnitude of the daytime biases is higher than either the overall biases
389 or nighttime biases.

390 For both outgoing and incoming radiation, daytime r^2 values and biases could be affected by
391 the delayed onset of daytime radiation in the models. Both models take an additional hour
392 before seeing increased incoming and outgoing solar radiation values, which is especially
393 visible following the frontal passage (Figure 4). The averaging of the hourly observations
394 when sunrise occurred in the middle of an hour may also contribute to the discrepancy
395 between the observations and simulations. Incoming solar radiation has much smaller biases.
396 The maximum daytime values reached 979 W/m^2 , leading to a maximum daytime average
397 bias of only 1%.

398 The nighttime data, in part, contributes to the increase in overall high r^2 of both incoming and
399 outgoing radiation when compared to the daytime values of the variables. Having this
400 underestimation of daytime solar insolation could explain the cool bias in the WRF model,
401 but does not explain the cool bias in the MM5 model.

402 Similar to the outgoing shortwave radiation, both models runs for incoming shortwave
403 radiation have larger postfrontal r^2 values (Table 5). Both of the models have comparable
404 postfrontal r^2 values, but WRF has higher prefrontal r^2 values. While WRF overestimated,
405 MM5 underestimated prior to the front, but both models overestimated similarly following
406 the front. WRF had the largest bias in the prefrontal cluster.

407

408 **3.2.2 Flux variables**409 *Latent heat flux*

410 The overall latent heat flux r^2 values for both simulations are even higher than for
411 temperature, but decrease when considering the daytime values and become almost negligible
412 when considering the nighttime values (Figure 5). WRF again has the highest r^2 values for
413 most of the groupings. When looking at the frontal passage period, the data tends to have a
414 high r^2 during the post-frontal period (Table 6).

415 In most cases the WRF model has a larger bias magnitude than the MM5 model (Table 6).
416 Overall and daytime latent heat flux is overestimated for both of the models with the largest
417 biases occurring during the daytime. The nighttime biases for both of the models are
418 relatively small. They are underestimated in MM5, but overestimated in WRF.

419 Prior to the frontal passage on August 29, latent heat values were scattered throughout the
420 day, which could correspond to lower moisture content (Figure 5). Following the frontal
421 passage (August 30 and 31), observed daytime latent heat flux increases, indicating increased
422 moisture. Both models overestimate daytime latent heat flux for the entire study period, but
423 WRF has larger overestimations than MM5 by approximately 20 W/m^2 (Table 6). However,
424 on August 30 and 31 both models perform similarly with overestimation biases of $\sim 21 \text{ W/m}^2$
425 and $\sim 17 \text{ W/m}^2$ for WRF and MM5, representing a difference of 6 W/m^2 . Both models vary
426 in their simulation of the meteorological conditions prior to the frontal passage but resort to
427 similar parameterizations following the front, perhaps in response to the clearer incoming
428 solar radiation simulations.

429

430 *Sensible heat flux*

431 WRF has higher overall, and daytime, values of r^2 compared to MM5, but has lower r^2 values
432 at night (Table 6). Both of the models had higher overall values compared to daytime
433 clustering, while the nighttime values are low. Compared to the diurnal r^2 , the r^2 is higher
434 both for all data and for the prefrontal and postfrontal clusters (Table 6).

435 For the study period there was an r^2 value of 0.49 between observed sensible heat flux and
436 water vapor mixing ratio at night. None of the models reach this level of r^2 values, but the
437 MM5 models get closer to this relationship than the WRF model. The decrease in r^2 from
438 sensible heat flux to latent heat flux and the decrease in the magnitude of the biases in MM5
439 are in agreement with the findings of Zhong et al. (2007). The WRF results agree with
440 LeMone et al. (2009), who found that their modeled sensible heat overestimated throughout

441 the entire study period, however our results show lower bias for sensible heat than latent heat,
442 which is in disagreement with the LeMone study. WRF had the highest overall, nighttime, and
443 daytime biases than MM5E. WRF and MM5E overestimated sensible heat flux for all clusters
444 with the exception of nighttime. While the r^2 decreased for sensible heat flux compared to
445 latent heat flux and the biases are smaller, the relative magnitude of the biases represents a
446 larger portion of measured values. During the daytime, MM5 had an average overestimation
447 of 2% while WRF overestimated by 38%. This is a 24% disparity between the values during
448 the daytime, but this gap decreases greatly at night, when WRF underestimated values by as
449 much as 0% while MM5 showed almost no bias.

450 The sensible heat flux shows similar simulation pattern to the latent heat flux time series
451 (Figure 5). During the first two days of the study period, both models respond differently to
452 the inconsistent sensible heat flux, but have similar responses during the two days following
453 the frontal passage. Overall, Figure 5 reflects the higher daytime biases for WRF compared
454 with MM5 (Table 6). Sensible heating is associated with ground heating, so it is possible that
455 temperature variations in the models, combined with differences in the moisture, could
456 contribute to these variations. However, the two days following the frontal passage produce
457 similar model responses, with WRF and MM5 overestimating sensible heat by $\sim 6 \text{ W/m}^2$.

458

459 *Ground flux*

460 Similar to the other flux variables, the overall r^2 values were higher than either the day or
461 nighttime values (Table 6). Out of all the flux variables, the overall and daytime r^2 values for
462 ground flux are the lowest. The nighttime r^2 values are also very low. The WRF model has
463 slightly higher r^2 values than the MM5 model overall and during the day, but is lower at night.
464 The ground flux biases do not follow the pattern that sensible and latent heat flux (Table 6).
465 During the day both models consistently underestimate for the entire study period as well as
466 for the two days following the frontal passage, and at night both models have similar
467 overestimations. Additionally, both models have similar timing of the ground flux that lies in
468 contrast with the observations (Figure 5). Both models have sharp increases of ground flux in
469 the evening that eventually diminish as the night progresses, while the observations have
470 gradual increases in ground flux through the afternoon and then sharp drops in the morning.
471 The ground flux is associated with increased ground temperatures as the sun reaches the
472 ground, so the increased insolation on the two days following the frontal passage leads to
473 slightly higher observed ground flux amplitudes. Both of the models capture these higher
474 ground flux values, but have higher amplitudes of both the amount of ground flux escaping

475 from and entering the ground, which again could be associated with the increased incoming
476 solar radiation found in the models.

477

478 **3.2.3 Turbulence**

479 Friction velocity, or u^* , is one measure of how much turbulence is being generated through
480 shearing forces at any given time (Stull, 1988). Examining the observed and modeled and
481 measured values can provide insight into shear turbulence that contributes to the development
482 of the PBL. Table 6 presents the overall and diurnal r^2 and bias values for friction velocity and
483 Figure 6 shows the time series for the study period.

484 Despite the fact that friction velocity is a small component of turbulent energy, the models are
485 able to model it relatively well with overall r^2 values of 0.73 and 0.70 for WRF and MM5,
486 respectively. The overall r^2 values for both of the models are higher than daytime values and
487 much higher than the nighttime values. At night, the models are set to a minimum value of 0.1
488 m/s, which does not always accurately reflect the observations that can get much smaller.
489 Above this threshold, both models attempt to mimic nighttime u^* behavior, but following the
490 frontal passage, nighttime wind speeds were relatively calm (Figure 3). On those nights
491 observed u^* values were well below the 0.1 m/s threshold, so neither model is able to
492 simulate these values, which could have led to the low nighttime r^2 values.

493 Both models overestimate u^* , which could be related to the overestimations in wind speed for
494 the models. There is no distinct cluster with the highest bias magnitudes; the largest bias for
495 WRF occurs during the daytime but for MM5 occurs at night. WRF has the highest overall,
496 daytime, and nighttime magnitude biases, which is in contrast with Hanna et al. (2010), who
497 mentioned that MM5 had larger biases in the afternoon than WRF. Friction velocity is a
498 measure of how much shear turbulence will be generated and is affected by topography and is
499 directly related to wind speed. Compared to the other model variables, the absolute biases for
500 friction velocity are relatively small, but assuming a maximum u^* value of approximately 0.6
501 m/s, the bias can be overestimated by nearly 30% in the WRF model.

502

503 **3.3 Planetary boundary layer**

504 Due to the small number of radiosonde launches available for the duration of the study period,
505 the biases were not calculated for planetary boundary layer height. However, PBL heights
506 were calculated at sunrise and sunset prior to the frontal passage, and then following the
507 frontal passage were recorded with more regularity, so the few observations available offer a
508 better chance to look at the development and destruction of the PBL (Figure 7). Ideally,

509 suppressed daytime temperatures and elevated nighttime temperatures should yield similar
510 PBL height results. However, while the daytime PBL heights are in fact underestimated
511 during the day as expected, they are also often underestimated at night when they should be
512 overestimated. Daytime peaks are better approximated following the frontal passage, but the
513 PBL destruction always happens too soon.

514 There are various reasons for the possible variations in the onset of PBL development and
515 destruction. Especially during the morning PBL height estimates, the late onset of solar
516 radiation in the models could contribute to the slow development of the PBL during a time
517 when convection leads to a rapid increase of PBL height. LeMone et al. (2009) suggests
518 overestimations of sensible heat lead to overestimations in the convective boundary layer
519 depth. In general, MM5E has the smallest underestimations and overestimations. However,
520 both models replicate PBL height estimations reasonably well, with a few exceptions though:
521 on August 29, both models do not capture the maximum PBL height, with WRF significantly
522 failing, while on September 1, MM5 performs quite well and WRF only reaches about 50% of
523 the observed PBL height.

524 Rappenglück et al. (2008) speculated whether PBL development was slower on ozone
525 exceedance days due to cooler temperatures delaying PBL development. In the postfrontal
526 environment temperatures were in fact cooler (Figure 3), but none of the models were able to
527 simulate temperature minimums for the nights of August 30 or 31. WRF gets closest to the
528 observed temperatures while MM5 has a larger bias following the front, which may explain
529 why MM5 overestimated noontime PBL height on August 30. WRF, however, besides getting
530 closer to early morning temperatures, underestimated daytime temperatures, which may
531 explain the underestimation of the PBL heights by WRF on August 31- September 01 (Figure
532 7). Increased PBL height allows for lower ozone concentrations, so it is no surprise that using
533 MM5 simulations as a meteorological driver for air quality modeling led to underestimation
534 of ozone on August 31 and September 01 by 25-30 ppb (Banta et al., 2011; Ngan et al, 2012).

535

536 **4. Conclusions**

537 Although WRF v3.5.1 does not perform as well as MM5 v3.6.1 in predicting PBL heights, it
538 does a better job in capturing energy budget and most of the general variables (with exception
539 of wind speed/direction and water vapor mixing ratio). Energy balance partitioning can have
540 an effect on standard and planetary boundary layer height variables. Both models
541 overestimate incoming solar radiation, which implies a surplus of energy that could be
542 exhibited in either the partitioning of the surface energy variables or in some other aspect of

543 the meteorological modeling not examined here. This scenario would also imply that there's
544 more energy available for the nighttime system, which should mean increased temperatures
545 and higher boundary layer height estimations. While nighttime temperatures do seem to
546 reflect this increased energy for both models, PBL height estimations only reflect it in WRF.
547 The nighttime temperature bias disparity in the models following the frontal passage could
548 reflect the disparity in moisture. The MM5 model consistently had much drier conditions than
549 the WRF model, which could mean more energy available to other parts of the meteorological
550 system. On the clearest day of the study period MM5 had increased latent heat flux, which
551 could lead to higher evaporation rates and lower moisture in the model. However, this latent
552 heat disparity between the two models is not visible during any other part of the study, so
553 examining sequential cloud-free days would be necessary to see whether the moisture and
554 latent heat effect was sustained. The full effects of moisture on the energy balance cannot be
555 determined here other than as a potential reason for inconsistent model outputs. The
556 difference in the land datasets used to initialize and update each model make this situation
557 plausible.

558 The frontal passage allowed this study to examine these variables both under prefrontal and
559 postfrontal conditions, and it was found that a frontal passage does affect the performance of
560 most of the variables, including the radiation, flux, and turbulence variables, at times creating
561 significant differences in the r^2 values. Ultimately the clear, sunny days offered the most
562 insight into the potential effects of the energy balance variables on standard variables and
563 planetary boundary layer height. These two days were also two of the highest 8-hour ozone
564 peak days on record for the year. Since these kinds of days are favorable for high ozone
565 production, the energy balance variables reproduced on these days could more accurately
566 represent meteorological conditions. Accurately determining the energy balance variables
567 could in turn produce better standard meteorology and PBL heights, which are essential in
568 determining accurate ozone concentrations.

569 The results presented in this paper are restricted to the validation of one 4-km domain grid
570 cell with observations in this specific grid cell. We do not claim that these validations are
571 valid throughout the domain and for each grid cell as this would require a corresponding
572 network of micrometeorological observations. However, we believe that a point-to grid
573 validation on one 4-km domain grid cell may still be helpful in elucidating different
574 behaviours and/or progresses in different models to simulate boundary layer properties.

575

576 **Acknowledgements**

577 We are grateful for financial and infrastructural support provided by the UH-CC and we like
578 to thank Dr. Fong Ngan (NOAA-ARL) for valuable discussions.
579

580 **References**

581 Air Resources Laboratory. Eta Data Assimilation System (EDAS) Archive Information.
582 <http://ready.arl.noaa.gov/edas80.php>. Accessed December 2, 2013.

583

584 Banta, R. M., C. Senff, J. Nielsen-Gammon, L. Darby, T. Ryerson, R. Alvarez, S. Spandberg,
585 E. Williams, and M. Trainer, 2005. A bad air day in Houston. *Bulletin of the American*
586 *Meteorological Society*, 86, 657-669.

587

588 Banta, R.M., C. Senff, R. Alvarez, A. Langford, D. Parrish, M. Trainer, L. Darby, R.
589 Hardesty, B. Lambeth, J. Neuman, W. Angevine, J. Nielsen-Gammon, S. Sandberg, and A.
590 White, 2011. Dependence of daily peak O₃ concentrations near Houston, Texas on
591 environmental factors: Wind speed, temperature, and boundary-layer depth. *Atmospheric*
592 *Environment*, 45, 162-173.

593

594 Borge, R., V. Alexandrov, J.J. del Vas, J. Lumberras, and E. Rodriguez, 2008. A
595 comprehensive sensitivity analysis of the WRF model for air quality applications over the
596 Iberian Peninsula. *Atmospheric Environment*, 42, 8560-8574.

597

598 Byun, D. W., and K. Schere, 2006. Review of the governing equations, computational
599 algorithms, and other componenets of the Models-3 community multiscale air quality
600 (CMAQ) modeling system. *Applied Mechanics Review*, 59, 51e77.

601

602 Chen, F., and J. Dudhia, 2001. Coupling an advanced land surface hydrology model with the
603 Penn State-NCAR MM5 modeling system. Part 1: Model implementation and sensitivity.
604 *Monthly Weather Review*. 129: 569-585.

605

606 Clements, C.B., Zhong, S., Goodrick, S., Li, J., Potter, B.E., Bian, X., Heilman, W.E.,
607 Charney, J.J., Perna, R., Jang, M., Lee, D., Patel, M., Street, S., and G. Aumann, 2007.
608 Observing the dynamics of wildland grass fires - FireFlux-A Field Validation Experiment.
609 *Bulletin of the American Meteorological Society*, 88, 1369-1382.

610

611 Cuchiara G.C., Li X., Carvalho J., and B. Rappenglück, 2014: Intercomparison of planetary
612 boundary layer parameterization and its impacts on surface ozone formation in the

613 WRF/Chem model for a case study in Houston/Texas, *Atmospheric Environment*, 96, 175-
614 185, <http://dx.doi.org/10.1016/j.atmosenv.2014.07.013>
615

616 Czader B.H., Li. X., and B. Rappenglück, 2013: CMAQ modeling and analysis of radicals,
617 radical precursors and chemical transformations, *J. Geophys. Res.*, 118, 11,376-11,387, doi:
618 10.1002/jgrd.50807
619
620

621 Day, B. M., R. Rappenglück, C. Clements, S. Tucker, and W. Brewer, 2010. Nocturnal
622 boundary layer characteristics and land breeze development in Houston, Texas during
623 TexAQS II. *Atmospheric Environment*, 44, 4014-4023.
624

625 Dudhia, J., 1989. Numerical study of convection observed during the winter monsoon
626 experiment using a mesoscale two-dimensional model. *Journal of the Atmospheric Sciences*,
627 46, 3077-3107.
628

629 Gilliam, R., and J. Pleim, 2010. Performance assessment of new land surface and planetary
630 boundary layer physics in the WRF-ARW. *Journal of Applied Meteorology and Climatology*,
631 49, 760-774.
632

633 Grell, G. A., J. Dudhia, and D. Stauffer, 1994. A description of the fifth-generation Penn
634 State/NCAR Mesoscale Model (MM5). NCAR Tech. Note NCAR/TN-3981STR, 122 pp.
635

636 Grell, G. A., and D. Devenyi, 2002. A Generalized approach to parameterizing Convection
637 combining Ensemble and Data Assimilation Techniques. *Geophysical Research Letters*, 29
638 (14), doi: 10.1029/2002GL015311.
639

640 Hanna, S.R. B. Reen, E. Hendrick, L. Santos, D. Stauffer, A. Deng, J. McQueen, M.
641 Tsudulko, Z. Janjic, D. Jovic, and R. Sykes, 2010. Comparison of Observed, MM5, and
642 WRF-NMM model-simulated, and HPAC-assumed boundary layer meteorological variables
643 for 3 days during the IHOP field experiment. *Boundary Layer Meteorology*. 134: 285-306.
644

- 645 Hong, S. Y., J. Dudhia, and S. H. Chen, 2004. A revised approach to ice microphysical
646 processes for the bulk parameterization of clouds and precipitation. *Monthly Weather*
647 *Review*, 132, 103-120.
- 648
- 649 Hong, S. Y., Y. Noh, and J. Dudhia, (2006). A New Vertical Diffusion Package with an
650 Explicit Treatment of Entrainment Processes. *Monthly Weather Review*, 2006, 2318 - 2341.
- 651
- 652 Hong, S. Y., and H. L. Pan, 1996. Nonlocal boundary layer vertical diffusion in a medium
653 range-forecast model. *Monthly Weather Review*, 124, 2322-2339.
- 654
- 655 Hu, X.M., J. Nielsen-Gammon, and F. Zhang, 2010. Evaluation of three planetary boundary
656 layer schemes in the WRF model. *Journal of Applied Meteorology and Climatology*. 49:
657 1831-1844.
- 658
- 659 Kain, J.S., 2004: The Kain–Fritsch convective parameterization: An update. *Journal of*
660 *Applied Meteorology*, 43, 170–181.
- 661
- 662 Kljun, N., Calanca, P., Rotach MW., and H.P. Schmid, 2004. A simple parameterisation for
663 flux footprint predictions, *Boundary Layer Meteorol.*, 112(3), 503–523,
664 doi:10.1023/B:BOUN.0000030653.71031.96.
- 665
- 666 Langford, A. O., S. Tucker, C. Senff, R. Banta, W. Brewer, R. Alvarez, R. Hardesty, B.
667 Lerner, and E. Williams, 2010. Convective venting and surface ozone in Houston during
668 TexAQS2006. *Journal of Geophysical Research*, 115, D16305.
- 669
- 670 LeMone, M., F. Chen, M. Tewari, J. Dudhia, B. Geerts, Q. Miao, R. Coulter, and R.
671 Grossman, 2009. Simulating the IHOP_2002 fair-weather CBL with the WRF-ARW-Noah
672 modeling system. Part 1: Surface fluxes and CBL Structure and evolution along the eastern
673 track. *Monthly Weather Review*. 138: 722-744.
- 674
- 675 Mao, Q., L.L. Gautney, T.M. Cook, M.E. Jacobs, S.N. Smith, and J.J. Kelsoe, 2006.
676 Numerical experiments MM5-CMAQ sensitivity to various PBL schemes. *Atmospheric*
677 *Environment*, 40: 3092-3110.
- 678

- 679 Mlawer, E. J., S. Taubman, P. Brown, M. Iacono, and S. Clough, 1997. Radiative transfer for
680 inhomogeneous atmosphere: RRTM, a validated correlated-k model for the longwave. *Journal*
681 *of Geophysical Research*, 102 (D14), 16663-16682.
- 682
- 683 Ngan, F., and D. Byun, 2011. Classification of weather patterns and associated trajectories of
684 high-ozone episodes in the Houston-Galveston-Brazoria area during the 2005/06 TexAQS-II.
685 *Journal of Applied Meteorology and Climatology*, 50, 485-499.
- 686
- 687 National Weather Service Environmental Modeling Center. NAM: The North American
688 Mesoscale Forecast System. <http://www.emc.ncep.noaa.gov/index.php?branch=NAM>.
689 Accessed November 24, 2013.
- 690
- 691 Ngan, F., D. Byun, H. C. Kim, D. G. Lee, B. Rappenglück, and A. Pour-Biazar, 2012.
692 Performance assessment of retrospective meteorological inputs for use in air quality modeling
693 during TexAQS 2006. *Atmospheric Environment*, 54: 86-96.
- 694
- 695 Rappenglück, B., R. Perna, S. Zhong, and G. Morris, 2008. An analysis of the vertical
696 structure of the atmosphere and the upper-level meteorology and their impact on surface
697 ozone levels in Houston, Texas. *Journal of Geophysical Research*, 113, D17315.
- 698
- 699 Skamarock, W.C., J. Klemp, J. Dudhia, D. Gill, D. Barker, M. Duda, X. Y. Hwang, and J.
700 Powers, 2008. A Description of the Advanced Research WRF Version 3. NCAR Tech Note
701 NCAR/TN-4751STR, 125 pp. [Available from UCAR Communications, P.O. Box 3000,
702 Boulder, CO 80307.]
- 703
- 704 Steenveld, G.J., M. Wokke, C. Zwaafink, S. Pijlman, B. Heusinkveld, A. Jacobs, and A.
705 Holtslag, 2010. Observations of the radiation divergence in the surface and its implication for
706 its parameterization in numerical weather prediction models. *Journal of Geophysical*
707 *Research*, 115, D06107.
- 708
- 709 Stull, R. B., 1988. An introduction to boundary layer meteorology. 13th Ed. Atmospheric and
710 Oceanographic Sciences Library. Springer Publishers.
- 711

- 712 Tucker, S.C., R. Banta, A. Langford, C. Senff, W. Brewer, E. Williams, B. Lerner, H.
713 Osthoff, and R. Hardesty, 2010. Relationships of coastal nocturnal boundary layer winds and
714 turbulence to Houston ozone concentrations during TexAQS 2006. *Journal of Geophysical*
715 *Research*, 115, D10304, doi: 10.1029/2009JD013169.
- 716
- 717 Wilczak, J.M., I. Djalalova, S. McKeen, L. Bianco, J. W. Bao, G. Grell, S. Peckham, R.
718 Mathur, J. McQueen, and P. Lee, 2009. Analysis of regional meteorology and surface ozone
719 during the TexAQS II field program and an evaluation of the NMM-CMAQ and WRF-Chem
720 air quality models. *Journal of Geophysical Research*, 114, D00F14.
- 721
- 722 Zhong, S., H.J. In, and C. Clements, 2007. Impact of turbulence, land surface, and radiation
723 parameterizations on simulated boundary layer properties in a coastal environment. *Journal of*
724 *Geophysical Research*, 112, D13110.
- 725

726

727 Table 1. Variable names and descriptions for the study.

728

729

Variable Name (Units)	Description
TEMP2 (°C)	Temperature at 2 m
Q2 (g/kg)	Water vapor mixing ratio at 2 m
WSPD10 (m/s)	Wind speed at 10 m
WDIR10 (deg)	Wind direction at 10 m
LHFLUX (W/m ²)	Latent heat flux at surface
SHFLUX (W/m ²)	Sensible heat flux at surface
GRNDFLUX (W/m ²)	Ground flux at surface
SWDOWN (W/m ²)	Shortwave incoming radiation at surface
LWDOWN (W/m ²)	Longwave incoming radiation at surface
SWUP (W/m ²)	Shortwave outgoing radiation at surface
USTAR (m/s)	Friction velocity
PBLH (m)	Planetary boundary layer height

730

731

732 Table 2. Radiosonde launch times (CST).

733

20060827	20060828	20060829	20060830	20060831	20060901
18:00	06:00 18:00	06:00 18:00	06:00 12:00 18:00	04:00 06:00 09:00 12:00 15:00 18:00 21:00	04:00 06:00 09:00 12:00 15:00
Total # Radiosondes: 20					

734

735

736

737 Table 3. Model simulation configurations.

738

Simulation	Model	PBL Scheme	LSM	Land Analysis
MM5E	MM5	MRF	Noah	EDAS
WRF	WRF-ARW	YSU	Noah	NAM

739

740

741

742

743 Table 4. Data clusters.

744

Cluster	Number Data Points
All	114
Daytime	64
Nighttime	50
Prefrontal	44
Postfrontal	70

745

746

747

748

749 Table 5. Results for r^2 and bias for all, diurnal, and frontal conditions for temperature (TEMP2), water vapor mixing ratio (Q2), wind speed
 750 (WSPD10), wind direction (WDIR), incoming longwave radiation (LWDOWN), Outgoing shortwave radiation (SWUP), and incoming shortwave
 751 radiation (SWDOWN).
 752

	TEMP2		Q2		WSPD10		WDIR10		LWDOWN		SWUP		SWDOWN	
	WRF	MM5E	WRF	MM5E	WRF	MM5E	WRF	MM5E	WRF	MM5E	WRF	MM5E	WRF	MM5E
r^2	0.78	0.56	0.37	0.73	0.28	0.40	0.02	0.29	0.52	0.64	0.87	0.52	0.89	0.81
r^2_{Day}	0.71	0.48	0.64	0.78	0.17	0.31	0.00	0.50	0.66	0.61	0.71	0.23	0.75	0.64
r^2_{Night}	0.57	0.04	0.10	0.66	0.09	0.45	0.09	0.03	0.31	0.47	-	-	-	-
r^2_{Prefront}	0.79	0.36	0.00	0.31	0.16	0.33	0.04	0.30	0.59	0.45	0.86	0.65	0.86	0.64
$r^2_{\text{Postfront}}$	0.79	0.65	0.00	0.56	0.44	0.45	0.06	0.27	0.15	0.48	0.88	0.76	0.91	0.92
Bias	0.24	0.23	-1.44	-2.61	1.70	0.18	-21.48	-2.41	0.34	3.00	8.22	33.23	43.70	9.56
Bias _{Day}	-0.71	-0.62	-1.47	-2.81	1.69	-0.11	-37.89	-8.32	-5.46	2.76	15.93	60.49	77.85	17.04
Bias _{Night}	1.46	1.33	-1.40	-2.36	1.72	0.54	-0.47	5.17	7.78	3.30	-1.66	-1.66	-0.01	-0.01
Bias _{Prefront}	0.59	-0.73	-1.32	-2.77	1.35	-0.08	-35.82	-10.23	6.16	4.35	11.27	79.12	61.38	-24.00
Bias _{Postfront}	0.02	0.84	-1.51	-2.51	1.93	0.34	-12.47	2.51	-3.31	2.15	6.29	4.38	32.58	30.65
RMSE	1.95	2.71	2.76	3.00	2.08	0.97	145.97	94.58	15.36	14.41	27.33	92.11	135.11	153.63
RMSE _{Day}	1.76	2.41	2.35	3.17	2.09	0.99	164.63	83.61	14.40	15.37	36.44	122.92	180.32	205.03
RMSE _{Night}	2.18	3.06	3.21	2.78	2.07	0.94	117.85	107.00	16.52	13.08	1.77	1.77	0.05	0.05
RMSE _{Prefront}	1.58	2.75	2.28	3.10	1.97	1.08	130.75	59.73	14.26	15.86	29.38	141.81	154.04	199.07
RMSE _{Postfront}	2.16	2.69	3.03	2.94	2.15	0.89	154.77	111.02	16.02	13.41	25.96	34.28	121.71	116.30

753

754

755

756 Table 6. Results for r^2 and bias for all, diurnal, and frontal conditions for latent heat flux (LHFLUX), sensible heat flux (SHFLUX), ground flux
 757 (GRNDFLUX), and friction velocity (USTAR).

758

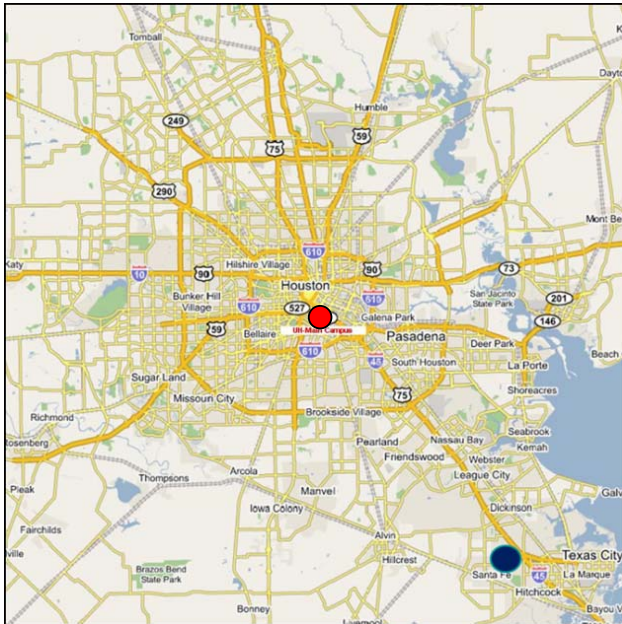
	LHFLUX		SHFLUX		GRNDFLUX		USTAR	
	WRF	MM5E	WRF	MM5E	WRF	MM5E	WRF	MM5E
r^2	0.88	0.87	0.89	0.77	0.68	0.67	0.73	0.70
r^2_{Day}	0.75	0.75	0.81	0.64	0.51	0.47	0.62	0.56
r^2_{Night}	0.37	0.00	0.08	0.16	0.03	0.13	0.26	0.11
r^2_{Prefront}	0.92	0.75	0.89	0.71	0.58	0.60	0.61	0.61
$r^2_{\text{Postfront}}$	0.89	0.92	0.90	0.81	0.74	0.70	0.81	0.77
Bias	42.31	26.99	14.32	3.75	-5.82	-10.52	0.15	0.02
Bias _{Day}	73.29	49.84	32.92	6.83	-46.70	-47.40	0.18	0.01
Bias _{Night}	2.65	-2.27	-9.48	-0.21	46.50	36.68	0.11	0.03
Bias _{Prefront}	60.96	16.46	21.00	5.39	-14.50	-15.72	0.15	0.00
Bias _{Postfront}	30.58	33.61	10.12	2.71	-0.37	-7.25	0.14	0.02
RMSE	77.77	70.62	38.89	31.5	60.85	56.09	0.17	0.08
RMSE _{Day}	103.7	94.04	50.76	41.52	69.33	66.35	0.20	0.08
RMSE _{Night}	5.18	7.11	12.29	7.48	47.86	39.23	0.14	0.06
RMSE _{Prefront}	94.26	74.02	40.94	35.30	56.22	49.93	0.19	0.09
RMSE _{Postfront}	65.32	68.40	37.55	28.86	63.59	59.64	0.16	0.07

759

760

761

762



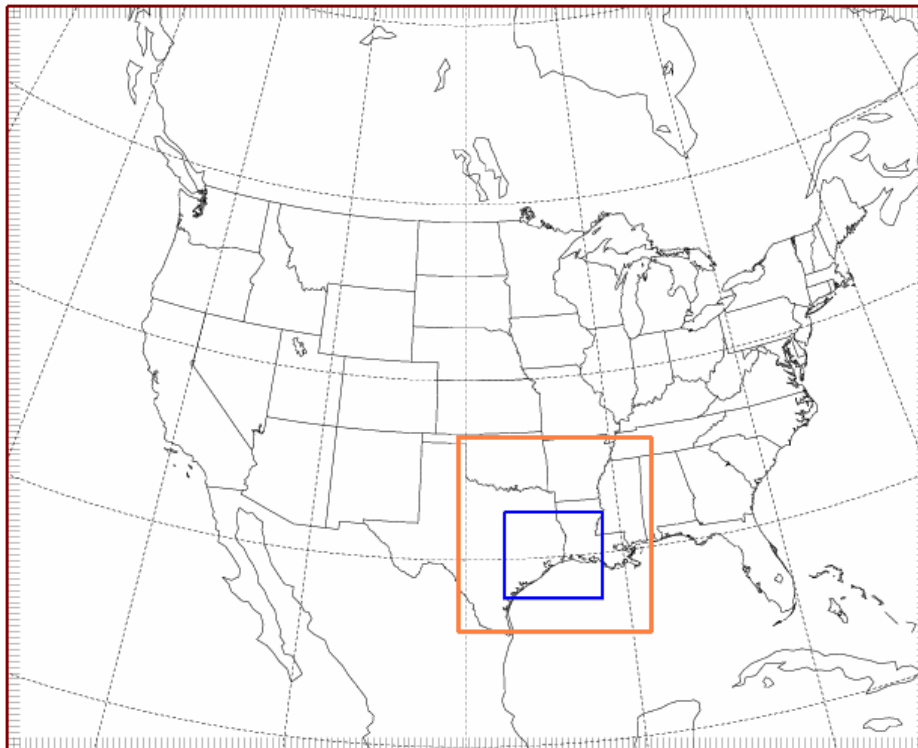
763

764 Figure. 1. Location of model and measurements. The dark blue dot represents the UH Coastal
765 Center and the red dot represents the UH Main Campus where the radiosondes were launched.

766

767

768



769

770 Figure. 2. Nesting domain for WRF and MM5 model. The blue box is the 4-km domain that
771 all model outputs were extracted from.

772

773

774

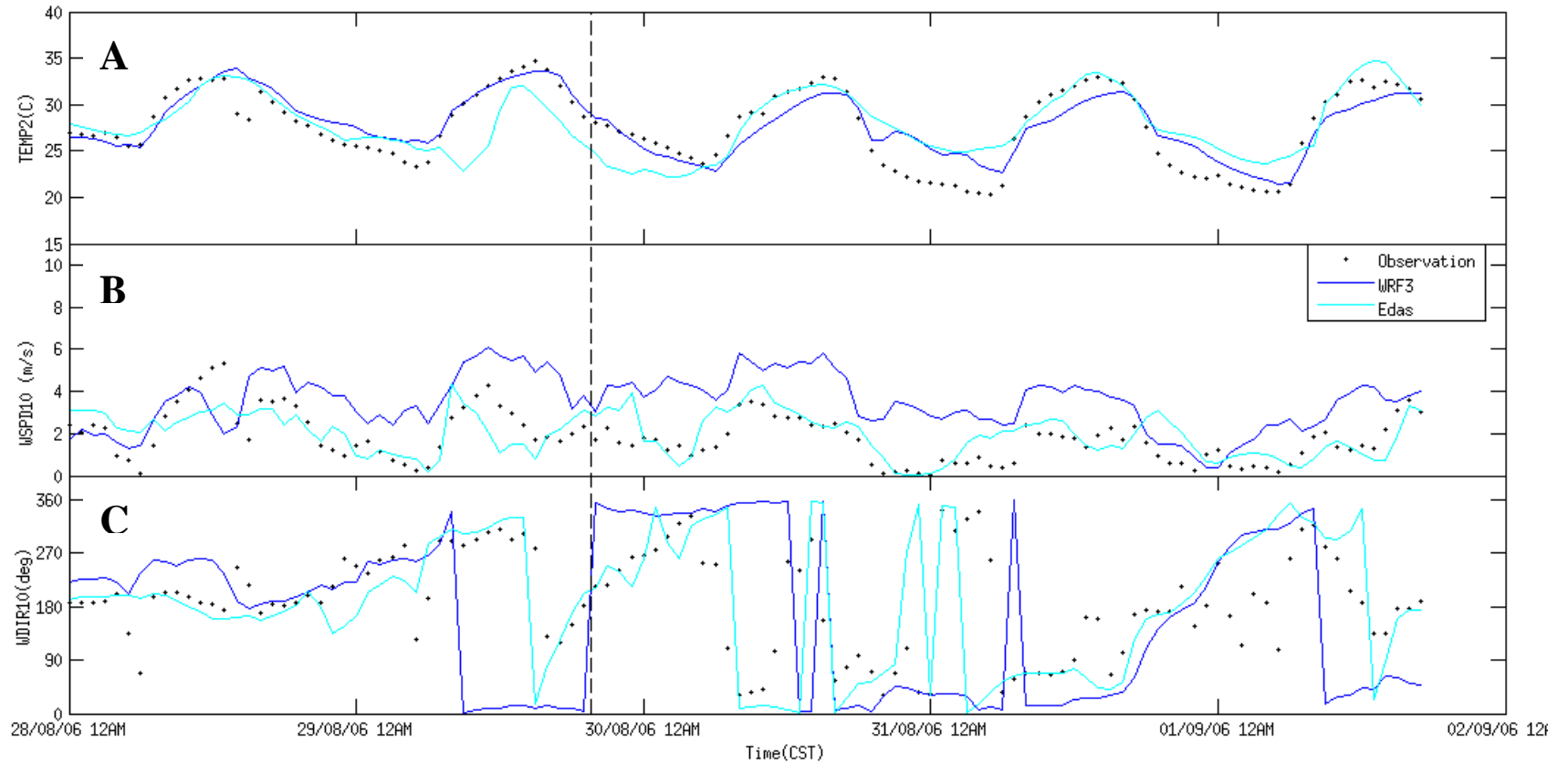
775

776

777

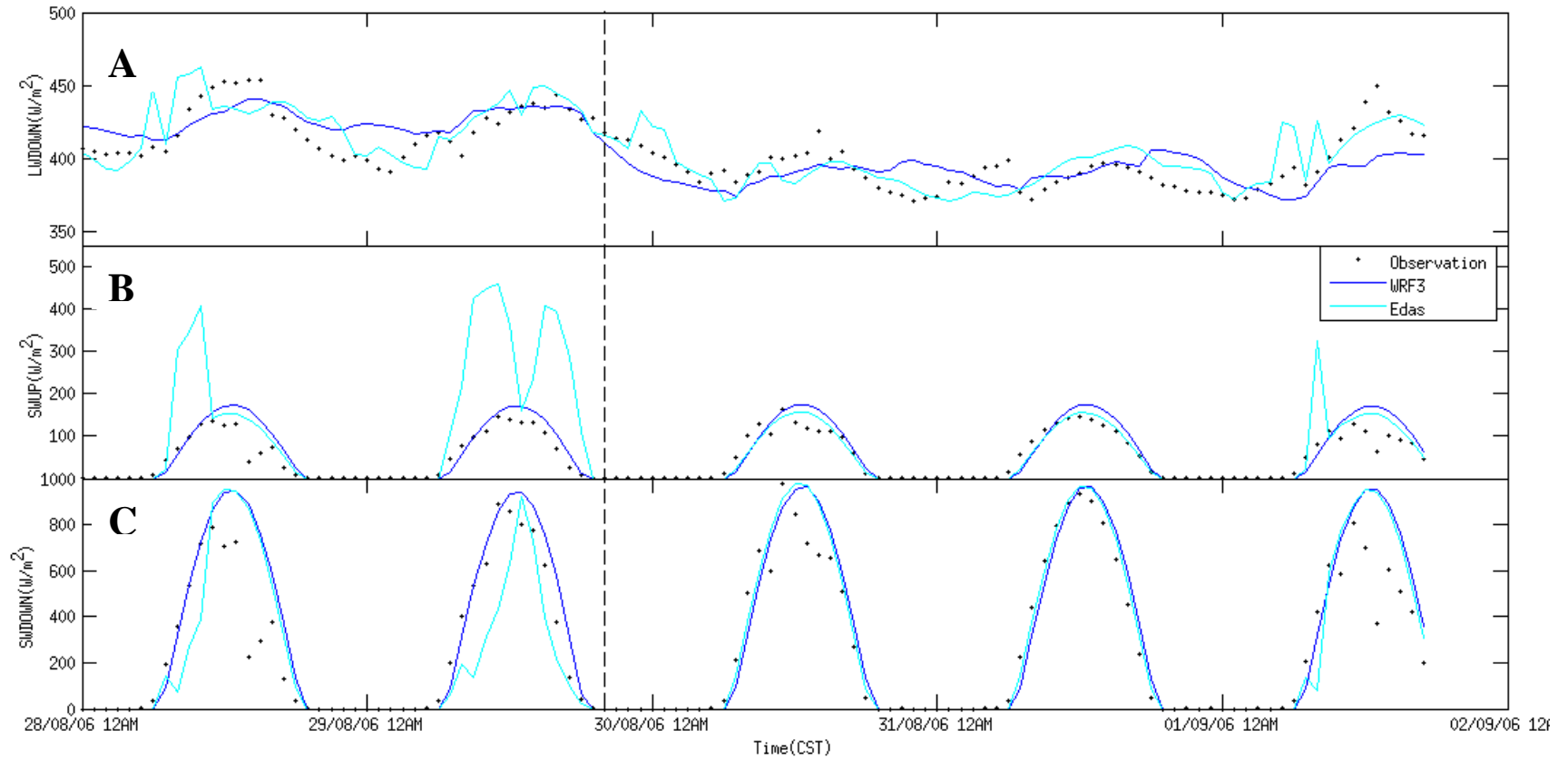
778

779



780

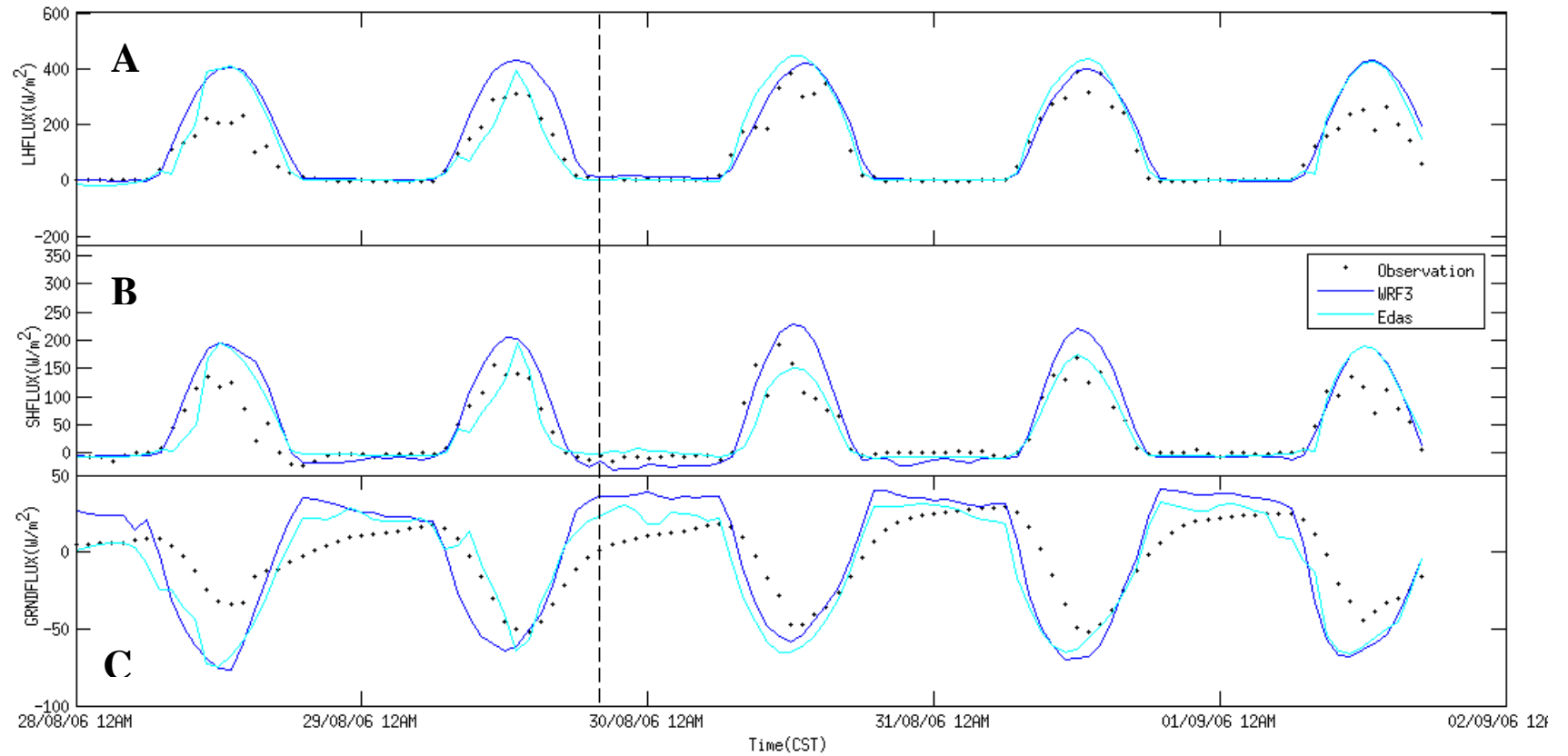
781 Figure. 3. Time series of temperature (A), wind speed (B), and wind direction (C) for observations (dots) and for the WRF (blue) and MM5 with
 782 EDAS (green) models. The dotted line marks the beginning of postfrontal conditions.



783

784 Figure. 4. Time series for incoming longwave (A), outgoing shortwave (B), and incoming shortwave (C) radiation for observations (dots) and for
 785 the WRF (blue) and MM5 with EDAS (green) models.

786



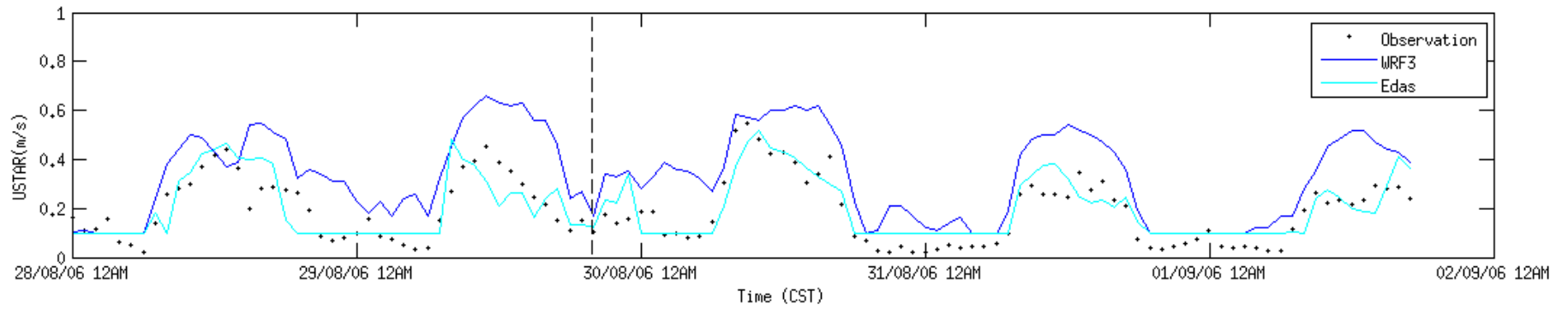
787

788 Figure. 5. Time series for latent heat (A), sensible (B), and ground (C) flux for observations (dots) and for the WRF (blue) and MM5 with EDAS
 789 (green) models.

790

791

792



793

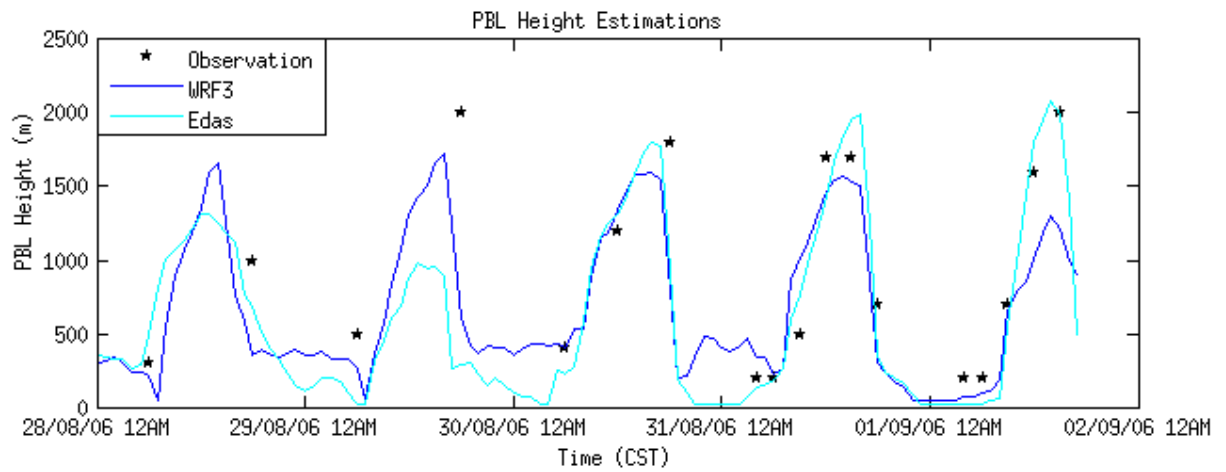
794

795 Figure. 6. Time series for friction velocity.

796

797

798



799

800

801 Figure. 7. Comparison of observed and simulated PBL height for the study period. The WRF
802 simulation tended to underestimate more than either of the MM5 simulations.

803

804